



Optics Letters

Dynamic modulation of nonreciprocal absorption in a graphene–InAs hybrid structure under low magnetic field and small incident angles

YE MING QING,^{1,2,*†} JIAO LIU,^{1,†} ZHAOYAN YANG,¹ LIANG WEI WU,^{2,3} YUE GOU,¹ JUN WU,^{4,5} AND BINGXIANG LI^{1,6}

¹College of Electronic and Optical Engineering & College of Flexible Electronics (Future Technology), Nanjing University of Posts and Telecommunications, Nanjing 210023, China

²State Key Laboratory of Millimeter Waves, Southeast University, Nanjing 210096, China

³School of Microelectronics, Hefei University of Technology, Hefei 230601, China

⁴College of Electrical Engineering, Anhui Polytechnic University, Wuhu 241000, China

⁵mailswj2011@163.com

⁶bxli@njupt.edu.cn

† These authors contribute equally to this work.

*ymqing@njupt.edu.cn

Received 18 December 2024; revised 22 January 2025; accepted 28 January 2025; posted 29 January 2025; published 20 February 2025

Overcoming Kirchhoff's laws to achieve strong nonreciprocity enhances energy harvesting and thermal management. Current magneto-optical (MO) strategies need high magnetic excitation and large incident angles, hindering practicality. We designed a graphene–InAs hybrid for significant nonreciprocity between absorptivity and emissivity at small angles with just 0.16 T, showing practical potential. By tuning graphene's Fermi energy, nonreciprocity strength can be adjusted via resonance mode competition. This design offers new insights for dynamic nonreciprocal radiation devices under near-normal light and modest magnetic excitation, facilitating practical use. © 2025 Optica Publishing Group. All rights, including for text and data mining (TDM), Artificial Intelligence (AI) training, and similar technologies, are reserved.

<https://doi.org/10.1364/OL.553323>

Kirchhoff's law establishes a foundational equivalence between spectral emissivity and absorptivity, asserting their identity under specific conditions. This reciprocal relationship provides a direct means of ascertaining an object's spectral emissivity through its absorptivity [1–4]. However, absorbed energy necessitates equivalent emission, reducing light collection efficiency. To overcome this and improve efficiency and thermal management, nonreciprocal radiation, independently modulating absorption and emission, is promising.

Numerous strategies have been proposed to realize nonreciprocal absorption, encompassing the integration of magnetic materials, time-varying, or nonlinear media within nanophotonic frameworks [5–17]. A seminal contribution was made by Zhu and Fan, who theoretically demonstrated nonreciprocal radiation utilizing a grating structure composed of InAs, a magneto-optical (MO) material, under a substantial 3 T magnetic field [18]. Yet, the practical implementation of such magnetic field conditions remains challenging. Consequently,

Zhao *et al.* introduced an innovative design where InAs was interposed between a grating-structured SiC and a metal plate, enabling nonreciprocal radiation under a reduced magnetic field of 0.3 T [19]. Li *et al.* studied a Si/InAs/Ag metamaterial for nonreciprocal thermal radiation under a magnetic field of 0.9 T [20]. Wu *et al.* introduced a nanophotonic design capable of achieving robust nonreciprocal radiation in the presence of a magnetic field of 2 T [21]. Chen *et al.* investigated an innovative design featuring a metal–SiC grating positioned atop a InAs film, enabling the realization of significant nonreciprocal thermal radiation near the normal direction under a modest magnetic field of 0.3 T [22]. Shayegan *et al.* experimentally observed the violation of Kirchhoff's law of thermal radiation by directly measuring the inequality between spectral directional emissivity and absorptivity in InAs-based structures [23]. Liu *et al.* experimentally demonstrated broadband mid-infrared nonreciprocal absorption using gradient epsilon-near-zero InAs thin films under a moderate magnetic field [24]. Despite these advancements, most current nonreciprocal emitters based on InAs still require external magnetic fields ranging from 0.3 to 3 T [20,22,25–27]. Therefore, further research is needed to explore methods for mitigating these magnetic field requirements and enhancing the practicality of InAs-based nonreciprocal systems.

Lambert's cosine law states that directional radiation energy intensity is proportional to the cosine of the angle θ between incident light and the surface normal. Minimizing θ maximizes radiation energy, enhancing light collection and measurement precision [28]. However, robust nonreciprocal designs often require high incidence angles ($\theta > 20^\circ$, sometimes $\theta > 80^\circ$) [9,21,25,29], reducing energy and precision. Current devices also lack dynamic tuning, crucial for performance optimization. Thus, innovative designs that achieve small incidence angles and dynamic tuning are urgently needed to improve nonreciprocal systems' practicality, performance, and versatility.

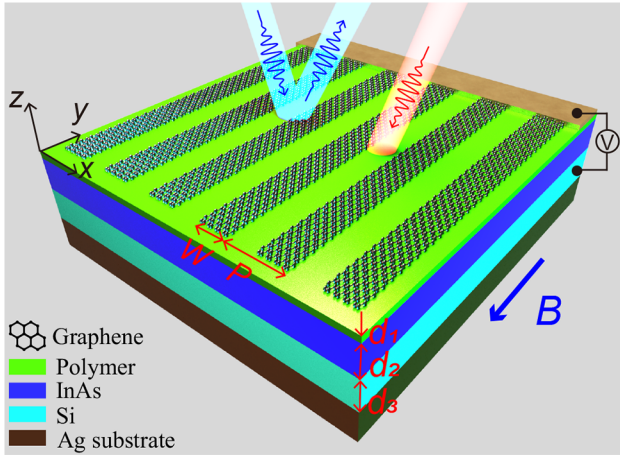


Fig. 1. Schematic diagram of the nonreciprocal graphene–InAs structure.

In this study, we propose a hybrid graphene–InAs structure capable of achieving strong nonreciprocal absorption. The proposed hybrid structure exhibits several notable advantages in miniaturization and integration. Primarily, it achieves strong nonreciprocal absorption under minimal external magnetic field conditions (0.16 T) and at small incident angles ($<10^\circ$), which is favorable for compact device designs. Additionally, the structure leverages localized plasmons in graphene and competitive mechanisms among multiple modes, enabling dynamic modulation of nonreciprocity with a modulation amplitude close to 0.9. This feature facilitates active tuning and enhances the versatility of the device for integration into various systems.

Figure 1 illustrates the proposed structure, which consists of (bottom to top) a Ag substrate, a Si layer, an InAs layer, a polymer layer, and a periodic array of graphene ribbons. The default geometric parameters for this structure are set as $P = 2 \mu\text{m}$, $W = 0.8 \mu\text{m}$, $d_1 = 0.1 \mu\text{m}$, $d_2 = 1.5 \mu\text{m}$, and $d_3 = 2 \mu\text{m}$, respectively. To evaluate the electromagnetic response of the hybrid graphene–InAs metasurface, we utilize the rigorous coupled wave analysis (RCWA) method with sufficient diffraction orders (e.g., 100). The dielectric constant for Si is 11.7 [30]. The polymer employed is conventional NFC (the dielectric constant is 2.4), a derivative of polyhydroxystyrene, which is commonly utilized as a planarizing underlayer in photolithographic processes [31]. The structure can be prepared as follows: the silicon layer can be deposited on the silver mirror by magnetron sputtering, while the InAs layer is prepared using a VG Semicon V90 MBE system [24]. The NFC layer is spin-coated on the InAs, and then large-scale graphene grown on copper foil by chemical vapor deposition is transferred to the NFC layer, and the desired structure is formed by electron beam lithography and oxygen plasma etching. The permittivity of Ag (ϵ_{Ag}) is determined by employing the Drude model [32]: $\epsilon_{\text{Ag}} = \epsilon_\infty - \omega_p^2 / (\omega^2 + j\omega\Gamma)$, where $\epsilon_\infty = 3.4$, $\Gamma = 2.7 \times 10^{13}$ rad/s, and $\omega_p = 1.39 \times 10^{16}$ rad/s. In the infrared frequency range, the equivalent permittivity of the graphene monolayer can be approximated using a Drude-like model [33]: $\epsilon_g = 1 + i\sigma_g / (\epsilon_0\omega t_g)$. Its equivalent permittivity (ϵ_g) is represented in terms of the angular frequency (ω), the vacuum permittivity (ϵ_0), the thickness of the graphene monolayer ($t_g = 0.34$ nm), and the surface conductivity $\sigma_g = ie^2 E_f / \pi \hbar^2 (\omega + i\tau^{-1})$, where τ is the carrier relaxation time. It is worth mentioning that the conductivity of this material

is significantly influenced by the Fermi energy (E_f), which is set to 0.1 eV by default in our study. This Fermi energy can be deliberately adjusted by applying a gate voltage to induce a static electric field or by using chemical doping methods. Unless stated otherwise, all other graphene parameters align with those established in our previous work [33]. To excite graphene plasmons, we only consider obliquely incident TM polarized light with an incident angle of θ . The dielectric constant tensor of InAs is described as follows [19]:

$$\epsilon_{\text{InAs}} = \begin{bmatrix} \epsilon_{xx} & 0 & \epsilon_{xz} \\ 0 & \epsilon_{yy} & 0 \\ \epsilon_{zx} & 0 & \epsilon_{zz} \end{bmatrix}, \quad (1)$$

where

$$\epsilon_{xx} = \epsilon_{zz} = \epsilon_\infty - \frac{\omega_p^2 (\omega + i\Gamma)}{\omega [(\omega + i\Gamma)^2 - \omega_c^2]}, \quad (2)$$

$$\epsilon_{xz} = -\epsilon_{zx} = i \frac{\omega_p^2 \omega_c}{\omega [(\omega + i\Gamma)^2 - \omega_c^2]}, \quad (3)$$

$$\epsilon_{yy} = \epsilon_\infty - \frac{\omega_p^2}{\omega (\omega + i\Gamma)}, \quad (4)$$

where ϵ_∞ , representing the high-frequency permittivity, is 12.37, and Γ , signifying the relaxation rate, amounts to 1.55×10^{11} rad/s. The plasma frequency, ω_p , is determined by the formula $\omega_p = \sqrt{n_e e^2 / (m^* \epsilon_0)}$, with $n_e = 7.8 \times 10^{17} \text{ cm}^{-3}$ being the free electron carrier density and $m^* = 0.033m_e$ (m_e is the electron mass). Additionally, $\omega_c = eB/m^*$ is the cyclotron frequency, where B represents the external magnetic field. Obviously, reciprocity is broken since $\epsilon_{xz} \neq \epsilon_{zx}$. The nonreciprocity of the system can be described as follows [8,24]:

$$\eta(\theta) = |\alpha(\theta) - e(\theta)|, \quad (5)$$

where $\alpha(\theta) = 1 - R(\theta)$, $e(\theta) = 1 - R(-\theta)$, and $R(\theta)$ are the absorptivity, emissivity, and reflectivity, respectively. The silver substrate is sufficiently thick (e.g., 1 μm) that the transmittance is zero, resulting in the incident wave being reflected or absorbed.

The absorptivity, emissivity, and nonreciprocal radiation spectra for $B = 0.16$ T at $\theta = 9^\circ$ are calculated and plotted in Fig. 2(a). A prominent emission resonance peak nearing unity can be distinctly observed, whereas the absorptance at its corresponding resonant wavelength (i.e., 24.15 μm) is merely 0.09.

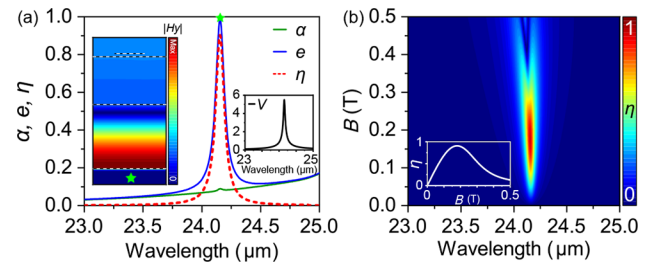


Fig. 2. (a) Absorptivity (lower-peaked solid curve), emissivity (higher-peaked solid curve), and nonreciprocity (dashed curve) as functions of the wavelength, under conditions where $\theta = 9^\circ$ and $B = 0.16$ T. The left inset shows the magnetic field distribution corresponding to the resonance peak. The right inset shows the $V = |\epsilon_{xz}|/|\epsilon_{xx}|$ as a function of the wavelength when the external magnetic field is 0.16 T. (b) Calculated nonreciprocity versus wavelength and magnetic field. The inset shows the variation of the nonreciprocal intensity with the applied magnetic field at an incident wavelength of 24.15 μm .

This disparity leads to a significant nonreciprocal radiation peak with an intensity reaching 0.9. The strength of the MO effect is related to $V = |\epsilon_{xz}|/|\epsilon_{xx}|$, as shown in the right inset of Fig. 2(a). It is evident that a prominent peak emerges at 24.15 μm , reaching an amplitude of 5.5, which significantly surpasses that reported in other work [34]. This indicates a strong MO property at this position, favorable for the realization of nonreciprocal effects. To gain an intuitive understanding of the resonance mechanism involved, we can consider the nonreciprocity of one single InAs slab atop of the silver layer. The Fabry–Perot (FP) resonance condition can be written as [34,35] $2k_z d_2 + 2\varphi_a + 2\varphi_s = 2\pi m$, where $2\varphi_a$ and $2\varphi_s$ are the phases of reflection coefficients r_a and $-r_s$ (i.e., the phase shifts for reflection of the light at the InAs–air and InAs–substrate interfaces), m is an integer, d_2 is the thickness of the InAs layer, and $k_z = \sqrt{(\omega/c)^2(\epsilon_{xx} - \epsilon_{xz}^2/\epsilon_{xx}) - k_x^2}$ is the wave vectors along the z axis. Consequently, the significant MO effect of InAs at specific wavelengths, in conjunction with the cavity resonance, collectively contributes to the nonreciprocal effect observed at small magnetic field and angle. We further computed the magnetic field distribution at this wavelength, as depicted in the left inset of Fig. 2(a). Notably, a distinct standing wave field is formed in the bottom Si layer, exhibiting a typical FP resonance [36,37]. In addition, it is crucial to highlight that the applied magnetic field significantly influences the optical properties of InAs, subsequently affecting the system's nonreciprocal characteristics, as illustrated in Fig. 2(b). It is evident that the system maintains good nonreciprocal properties within a certain magnetic field range. Specifically, the nonreciprocal intensity remains above 0.8 in the magnetic field range of 0.12–0.24 T. This demonstrates a notable advantage of this structure: compared to most other InAs-based nonreciprocal structures, it requires a smaller external magnetic field, rendering it more practical for real-world applications.

We further investigated the impact of several key structural parameters on the absorptivity, emissivity, and nonreciprocal coefficient. As illustrated in Fig. 3(a), the period of the graphene strips exerts minimal influence on the system. This can be attributed to the fact that cavity resonance phenomena are primarily determined by the longitudinal optical path length, where the transverse period is not a crucial factor in forming resonances. Moreover, for the localized plasmon resonances of graphene strips (whose resonance wavelengths are associated with their strip widths and Fermi levels [38,39], i.e., $\lambda \propto \sqrt{W/E_f}$), the width of the graphene strips is a significant factor rather than the period. We delved deeper into the effects of graphene strip dimensions, as depicted in Fig. 3(b). It is noteworthy that when the Fermi level of graphene is set to 0.1 eV, the excitation efficiency of graphene localized plasmons is low within the range of stripe width adjustments; hence, no pronounced changes are observed. However, when the graphene energy level is set to 0.33 eV, as shown in the inset of Fig. 3(b), a clear excitation of graphene localized plasmons is evident (as indicated by the electric field distribution in the inset). As the strip width increases, the resonance wavelength also increases, eventually overlapping with the FP mode at specific locations, leading to significant mode competition. This, in turn, results in a gap in the nonreciprocal spectrum. As demonstrated in Fig. 3(c), we examined the influence of the Si layer thickness. Clearly, variations in the Si layer thickness alter the optical path difference for light propagating back and forth within the cavity, thereby affecting the phase difference and leading to changes in interference effects. This

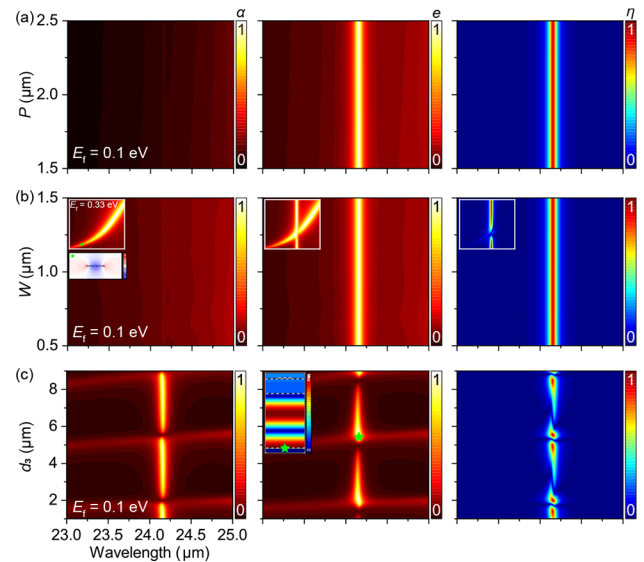


Fig. 3. Variations of absorptivity, emissivity, and nonreciprocity for variation of geometric parameters: (a) grating period P , (b) graphene strip width W , and (c) Si spacer thickness d_3 . In each case, other parameters are not changed. The insets in (b) show the effect of varying the graphene strip at a graphene Fermi energy of 0.33 eV. The star marks the field intensity distribution near the graphene at this location. The inset in (c) shows the magnetic field distribution corresponding to the resonance peak.

subsequently influences the FP resonance effects (as different orders of FP modes are also shown in the inset), resulting in a pronounced periodic variation in absorption, emission, and nonreciprocity.

The adjustment of the aforementioned structural parameters allows for passive modulation of nonreciprocal characteristics. However, in practical applications, once the device is fabricated, its structure becomes fixed. Therefore, exploring active modulation methods warrants further investigation. Figure 4(a) illustrates the impact of the incidence angle on nonreciprocal characteristics, revealing that the resonance positions of absorption and emission peaks are almost unaffected by the incidence angle (as shown in the inset), demonstrating notable angle-insensitive properties. As shown in Fig. 4(b), the system maintains good nonreciprocal characteristics within a certain angular range; specifically, it can sustain a nonreciprocal intensity above 0.8 within a 5.7° range and above 0.5 within a 12.5° range. This characteristic renders it applicable to wide-angle thermal emitters, communication systems, and sensing devices. Moreover, the angles that exhibit better nonreciprocal responses are all less than 20° , showcasing favorable small-angle response characteristics.

Lastly, we also investigated the influence of the Fermi level of graphene, as depicted in Fig. 4(c). Evidently, the resonance wavelength of graphene localized plasmons decreases with the increase in the graphene Fermi level (as shown in the inset), which aligns with theoretical expectations. Notably, when the Fermi level increases to approximately 0.3 eV, graphene localized plasmons compete with the FP cavity mode and gradually dominate in this competition, leading to a weakening of nonreciprocal characteristics. The specific physical changes are presented in Fig. 4(d), where it can be observed that as the Fermi level increases to 0.33 eV, the nonreciprocal intensity

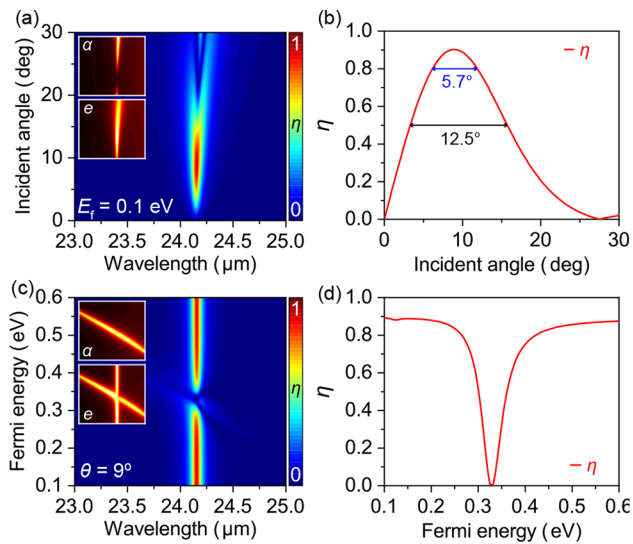


Fig. 4. (a) Calculated nonreciprocity versus wavelength and incident angle. The insets show the corresponding changes in absorptivity and emissivity. (b) Spectral nonreciprocity versus the incident angle at $24.15 \mu\text{m}$. (c) Calculated nonreciprocity versus the change of both the wavelength and graphene Fermi energy. The insets show the corresponding changes in absorptivity and emissivity. (d) Spectral nonreciprocity versus the graphene Fermi energy at $24.15 \mu\text{m}$.

undergoes a significant peak–valley transition, followed by a gradual increase in nonreciprocity. Hence, by leveraging the mode competition mechanism, dynamic modulation of nonreciprocal intensity can be achieved, with a modulation amplitude close to 0.9, enabling dynamic switching from a strongly nonreciprocal state to a reciprocal state. This finding holds significant value for the development of active nonreciprocal devices. Liu *et al.* have experimentally demonstrated that InAs-based resonant structures can achieve nonreciprocal radiation [24]. Therefore, we can use the same approach to perform our measurements. The reflectivity spectrum was measured in a custom-built infrared MO Kerr effect characterization setup. A Fourier transform infrared spectrometer generates broadband infrared light, reflected and deflected by mirrors, focused onto the sample, and then detected. A magnet applies an adjustable magnetic field (up to 2 T), with intensity measured by a gaussmeter. Background calibration involves measuring a gold-coated silicon wafer’s reflectivity, normalizing the sample’s spectrum. Graphene regulation is achieved by adjusting its gate voltage.

In summary, we have successfully designed and analyzed a novel graphene–InAs hybrid structure that demonstrates strong nonreciprocal absorption under minimal external magnetic field conditions (0.16 T) and at small incident angles ($<10^\circ$). By harnessing the localized plasmons in graphene and leveraging competitive mechanisms among multiple modes within the hybrid system, we have achieved dynamic modulation of nonreciprocal intensity. This design outperforms existing InAs-based structures, reducing magnetic field needs and improving small-angle response. It maintains good nonreciprocal properties within specific ranges, showing practical potential. By tuning the graphene Fermi level, we demonstrated near-0.9 mod-

ulation amplitude between nonreciprocal and reciprocal states. This innovation offers insights for dynamically tunable devices, enhancing thermal management and light collection efficiency. The hybrid structure promises future research and practical implementation in nonreciprocal radiation.

Funding. National Natural Science Foundation of China (62305173, 62405142, 62401191); Natural Science Research of Jiangsu Higher Education Institutions of China (23KJB140015); State Key Laboratory of Millimeter Waves (K202433); Youth Talent Support Program of the Jiangsu Association for Science and Technology (JSTJ- 2024-390).

Disclosures. The authors declare no conflicts of interest.

Data availability. Data underlying the results presented in this paper are not publicly available at this time but may be obtained from the authors upon reasonable request.

REFERENCES

- D. G. Baranov, Y. Xiao, I. A. Nechepurenko, *et al.*, *Nat. Mater.* **18**, 920 (2019).
- S. Fan, *Joule* **1**, 264 (2017).
- M. F. Picardi, K. N. Nimje, and G. T. Papadakis, *J. Appl. Phys.* **133**, 111101 (2023).
- W. Li and S. Fan, *Opt. Express* **26**, 15995 (2018).
- S. Yang, M. Liu, C. Zhao, *et al.*, *Nat. Photonics* **1**, 412 (2024).
- B. Zhao, J. Wang, Z. Zhao, *et al.*, *Phys. Rev. Appl.* **16**, 064001 (2021).
- D. L. Sounas and A. Alù, *Nat. Photonics* **11**, 774 (2017).
- Y. M. Qing and J. Wu, *Results Phys.* **60**, 107657 (2024).
- X. Shi and B. Wang, *Appl. Phys. Lett.* **125**, 062202 (2024).
- J. Fang, M. Wang, J. Yue, *et al.*, *Int. Commun. Heat Mass Transfer* **148**, 107031 (2023).
- Z. Luo, M. Z. Chen, Z. X. Wang, *et al.*, *Adv. Funct. Mater.* **29**, 1906635 (2019).
- J. Wu and Y. M. Qing, *Appl. Phys. Lett.* **121**, 112201 (2022).
- C. Guo, V. S. Asadchy, B. Zhao, *et al.*, *eLight* **3**, 2 (2023).
- J. Wu and Y. M. Qing, *Appl. Phys. Lett.* **122**, 012203 (2023).
- B. Zhao, C. Guo, C. A. C. Garcia, *et al.*, *Nano Lett.* **20**, 1923 (2020).
- Z. Wang, S. Xu, G. Zheng, *et al.*, *Opt. Lett.* **49**, 262 (2024).
- X. Wu, H. Yu, F. Wu, *et al.*, *AIP Adv.* **11**, 075106 (2021).
- L. Zhu and S. Fan, *Phys. Rev. B* **90**, 220301 (2014).
- B. Zhao, Y. Shi, J. Wang, *et al.*, *Opt. Lett.* **44**, 4203 (2019).
- J. Li, B. Wang, and J. Wu, *Appl. Mater. Today* **39**, 102345 (2024).
- X. Wu, Z. Chen, and F. Wu, *ES Energy Environ.* **13**, 8 (2021).
- Z. Chen, S. Yu, C. Yuan, *et al.*, *Int. J. Heat. Mass Transf.* **222**, 125202 (2024).
- K. J. Shayegan, S. Biswas, B. Zhao, *et al.*, *Nat. Photonics* **17**, 891 (2023).
- M. Liu, S. Xia, W. Wan, *et al.*, *Nat. Mater.* **22**, 1196 (2023).
- K. J. Shayegan, B. Zhao, Y. Kim, *et al.*, *Sci. Adv.* **8**, eabm4308 (2022).
- J. Wu and Y. M. Qing, *J. Chem. Phys.* **159**, 224701 (2023).
- J. Wu and Y. M. Qing, *Adv. Compos. Hybrid Mater.* **6**, 87 (2023).
- M. A. Green, *Nano Lett.* **12**, 5985 (2012).
- J. Wang, K. Shi, and X. Xing, *Mater. Today Phys.* **46**, 101515 (2024).
- M. Wang, Y. Yu, S. Prucnal, *et al.*, *Nanoscale* **14**, 2826 (2022).
- D. B. Farmer, H.-Y. Chiu, Y.-M. Lin, *et al.*, *Nano Lett.* **9**, 4474 (2009).
- B. Zhao and Z. M. Zhang, *J. Quant. Spectrosc. Radiat. Transfer* **135**, 81 (2014).
- Y. M. Qing, H. F. Ma, and T. J. Cui, *ACS Photonics* **6**, 2884 (2019).
- X. Wu, R. Liu, H. Yu, *et al.*, *J. Quant. Spectrosc. Radiat. Transfer* **272**, 107794 (2021).
- S. Dai, Z. Fei, Q. Ma, *et al.*, *Science* **343**, 1125 (2014).
- Z. Li, S. Butun, and K. Aydin, *ACS Photonics* **2**, 183 (2015).
- Y. She, K. Zhong, M. Tu, *et al.*, *Photonics* **11**, 497 (2024).
- W. Gao, J. Shu, C. Qiu, *et al.*, *ACS Nano* **6**, 7806 (2012).
- Y. M. Qing, H. F. Ma, and T. J. Cui, *J. Opt. Soc. Am. B* **38**, 3206 (2021).